Available online at www.sciencedirect.com
ScienceDirect
Journal of Power Sources 164 (2007) 189–195
JOURNAL OF POWER SOURCES
www.elsevier.com/locate/jpowsour

Modeling water transport in liquid feed direct methanol fuel cells

Wenpeng Liu [a,*], Chao-Yang Wang [b]

[a] *MTI Micro Fuel Cells Inc., 431 New Karner Road, Albany, NY 12205, USA*
[b] *Electrochemical Engine Center (ECEC), Department of Mechanical and Nuclear Engineering, The Pennsylvania State University, University Park, PA 16802, USA*

Received 12 September 2006; received in revised form 10 October 2006; accepted 11 October 2006
Available online 13 November 2006

Abstract

Proper water management in direct methanol fuel cells (DMFCs) is very critical and complicated because of many interacting physicochemical phenomena. Among these, the liquid saturation in the cathode side is believed to have a very strong effect on water crossover through the membrane, a key parameter to determine water balance between the anode and cathode. In this paper, based on an interfacial liquid coverage model implemented in a three-dimensional (3D) two-phase DMFC model, the liquid saturation variations in the cathode are examined in detail and their effects on the net water transport coefficient through the membrane discussed.

Keywords: Direct methanol fuel cell; Water transport; Mathematical modeling; Three-dimension; Interfacial liquid coverage

1. Introduction

The direct methanol fuel cell (DMFC) is considered as a leading contender for next-generation portable and micro power sources, offering a combination of simplicity, robustness and high energy density. Recent research indicates that water management [1,2] is one of most critical challenges for DMFCs to compete with lithium-ion batteries.

Constrained by the methanol crossover problem, the anode fuel solution has been very dilute, meaning that a large amount of water needs to be carried in the system and therefore reducing the energy content of the fuel mixture. In addition, for each methanol molecular reacted in the anode catalyst, 16 water molecules will be lost from the anode, assuming that the electro-osmotic drag coefficient of water is equal to 2.5 per proton through a thick membrane, such as Nafion 117 [3]. On the other hand, inside the cathode, there are 15 water molecules transported from the anode and 3 additional water molecules produced by consuming 6 protons generated from oxidation of 1 methanol. How to minimize water removal from the cathode and subsequent recovery externally to replenish the anode without causing severe cathode flooding becomes an important engineering issue.

Formally, the net water flux through the membrane, caused by diffusion, electro-osmosis, and hydraulic pressure differential across the membrane, can be quantified in terms of the net water transport coefficient, expressed as $\alpha = N_m^{H_2O}/N^{H^+}$ [4,5]. The ideal water transport condition, i.e. a water neutral cell, can be achieved when $\alpha = -1/6$ [2]. In other words, no water is needed from the anode feed and one water molecule needed to oxidize methanol comes from the product water generated on the cathode side. The magnitude and spatial distribution of α are thus very important for the design of innovative water management strategies in DMFCs.

Based on the theory of liquid water transport in proton exchange membrane fuel cells (PEMFCs) [6,7], a unique MEA structure has been developed, which utilizes a thin membrane (e.g. Nafion 112) to promote water back flow from the cathode to anode. Such MEAs exhibit extraordinarily low α and hence are generally termed low-α MEA technology [1,2,5].

Recent visualization data from H_2/air PEMFCs show that in the high current density and/or low gas flowrate conditions, water produced from the oxygen reduction reaction is removed from the GDL and gas channel in the liquid phase. Liquid water transport through hydrophobic GDL is driven by the gradient in capillary forces. At the hydrophobic surface of the GDL facing

* Corresponding author. Tel.: +1 518 533 2232; fax: +1 518 533 2223.
E-mail address: wliu@mechtech.com (W. Liu).

0378-7753/$ – see front matter © 2006 Elsevier B.V. All rights reserved.
doi:10.1016/j.jpowsour.2006.10.047

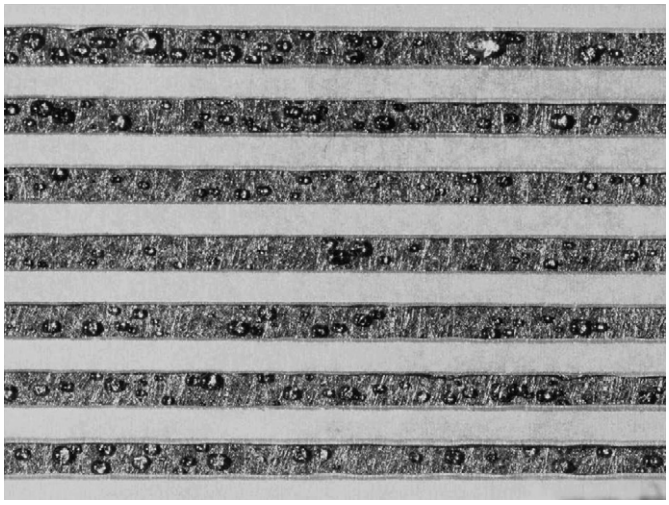

Fig. 1. Image of the cathode backing layer covered by water droplets in seven-channel flow field with a total active area of 3 cm^2 [8].

the gas channel, liquid water emerges in the form of droplets, as shown in the experimental image of Zhang et al. [8], which is reproduced here in Fig. 1. The droplet detachment diameter along with the droplet population density at the GDL surface will result in an interfacial liquid saturation, which is a key parameter to determine the level of flooding inside the GDL and catalyst layer. This same concept of interfacial coverage is believed to be important in a portable DMFC because much water exists in the DMFC cathode due to water crossover through the membrane.

In tandem with experimental water transport research, various mathematical models were also developed in order to achieve a deeper understanding of water behavior in the PEFC [6,7,9]. However, mathematical modeling of water transport in DMFCs has received little attention if any, due to the recognization of its importance only most recently. For the first time, Liu and Wang [10] presented a 3D, two-phase DMFC model, which includes flow channels, backing and catalyst layers on both anode and cathode sides, and the membrane as a single simulation domain, that elaborates water transport. This model is extended to further study the net water transport coefficient distribution and interfacial liquid water coverage effect in the present paper. A more complete review of DMFC modeling in the literature is recently given by Wang [11].

In the following, a 3D, two-phase mathematical model of DMFCs with the above-mentioned water transport features will be presented, and then solved by a commercial flow solver, Fluent®. Model results will be presented to illustrate the net water transport coefficient distribution in a 3D geometry and water transport behavior under different liquid water coverage conditions.

2. Physical model

The two-phase steady-state DMFC model in this work consists of non-linear, coupled partial differential equations of conservation of mass, momentum, species and charge. These can be presented in concise form as follows [10]:

$$\text{Continuity}: \quad \frac{\partial(\varepsilon\rho)}{\partial t} + \nabla\cdot(\rho\mathbf{u}) = \dot{m} \tag{1}$$

$$\text{Momentum}: \quad \frac{1}{\varepsilon}\left[\frac{\partial(\rho\mathbf{u})}{\partial t} + \frac{1}{\varepsilon}\nabla\cdot(\rho\mathbf{u}\mathbf{u})\right] = -\nabla p + \nabla\cdot\tau + S_{\mathbf{u}} \tag{2}$$

$$\text{Species}: \quad \frac{\partial c}{\partial t} + \nabla\cdot\{\gamma\mathbf{u}c\} = \nabla\cdot[D^k_{\text{l,eff}}\nabla c^k_{\text{l}} + D^k_{\text{g,eff}}\nabla c^k_{\text{g}}] - \nabla\cdot\left[\left(\frac{c^k_{\text{l}}}{\rho_{\text{l}}} - \frac{c^k_{\text{g}}}{\rho_{\text{g}}}\right)\mathbf{j}_{\text{l}}\right] + S^k \tag{3}$$

$$\text{Proton transport}: \quad 0 = \nabla\cdot(\kappa_{\text{eff}}\nabla\Phi_{\text{e}}) + S_{\Phi} \tag{4}$$

where ρ, $\mathbf{u}$, c and Φ_{e} denote the two-phase mixture density, velocity vector, molar concentration of species k and electrolyte phase potential, respectively. The species considered here are methanol, water and oxygen. The various two-phase properties, source terms, electro-chemical kinetics and thermophysical properties identified for various regions of a DMFC, as well as necessary boundary conditions, have been detailed in refs. [10,12–14] and thus are not repeated here.

Liquid saturation is a key parameter in the two-phase flow model. Here, we can obtain the liquid saturation from the mixture water molar concentration via

$$s = \frac{c^{\text{H}_2\text{O}} - c^{\text{H}_2\text{O}}_{\text{g,sat}}}{c^{\text{H}_2\text{O}}_{\text{l}} - c^{\text{H}_2\text{O}}_{\text{g,sat}}} \tag{5}$$

Zhang et al. [8,15] most recently found that the interfacial liquid saturation correlates strongly with the channel gas velocity as the droplet detachment diameter from the backing layer surface decreases with the gas velocity as a result of the balance between the drag force of air core flow on the drop and the drop's surface adhesion with the cathode backing layer. In addition, since liquid tends to form a droplet or a film at the hydrophobic and hydrophilic porous surfaces, respectively, the interfacial liquid saturation at the cathode backing layer and channel interface is also a function of the cathode backing layer wettability, i.e. contact angle. Furthermore, the droplet population density at the cathode backing layer surface, i.e. the number of sites activated with droplet emergence, is related to the local current density. Therefore, the interfacial liquid saturation is also a function of the current density. To summarize, we have

$$s_{\text{int}} = s(\mathbf{u}, \theta_{\text{c}}, i) \tag{6}$$

The exact form of this interfacial saturation function is to be determined by experimental measurements for a specific cathode porous material system. In the present 3D model focusing on exploring fundamental physics and numerical behaviors of two-phase dynamics with interfacial liquid coverage at the cathode backing layer surface, we implemented a constant interfacial liquid saturation for the purpose of a parametric study in this work.

Table 1
Three-dimensional cell geometry and operating conditions

Cell length (m)	0.1
Cell width (m)	2×10^{-3}
Anode channel width (m)	1×10^{-3}
Anode backing thickness (m)	300×10^{-6}
Anode catalyst thickness (m)	10×10^{-6}
Membrane thickness (m)	50×10^{-6}
Cathode catalyst thickness (m)	10×10^{-6}
Cathode backing thickness (m)	300×10^{-6}
Cathode channel width (m)	1×10^{-3}
Operating temperature (°C)	60
Anode channel pressure (atm)	1
Cathode channel pressure (atm)	1
Flow stoichiometry of anode channel	2
Flow stoichiometry of cathode channel	3
Inlet methanol concentration at anode (mol m^{-3})	2000 (2 M)
Inlet oxygen concentration at cathode (mol m^{-3})	7.68
Inlet liquid saturation at anode (%)	100
Inlet liquid saturation at cathode (%)	0 (fully humidified air)
Interfacial liquid saturation at the cathode backing layer (%)	0, 5, 10, 20
Cell operating voltage (V)	0.4

3. Results and discussion

As discussed, water transport through the membrane is governed by electro-osmotic drag, diffusion and hydraulic permeation. The electro-osmotic drag coefficient is only a function of temperature and thus a constant at any fixed operating cell temperature at steady state. Water diffusion and hydraulic permeation through the membrane are highly dependant on the liquid saturation of both anode and cathode sides. With the liquid coverage model applied at the interface of the cathode backing layer and flow channel, water diffusion driven by the water content gradient and water permeation by the hydraulic pressure gradient vary significantly and therefore, affect the net water transport coefficient, α, considerably.

The predictions of water crossover coefficient using a 1D version of the present model has been found to be in good agreement with experimental data [16], demonstrating the validity of this physical model. In the following, focus is placed on discussing 3D water transport simulation results for a 3D geometry and operating conditions described in Table 1. To clearly understand numerical results shown in this section, several representative planes in the 3D domain are described in Fig. 2 to facilitate the presentation of numerical results.

The liquid saturation distribution in the cathode backing layer without interfacial coverage is shown in several planes in Figs. 3–5. In this case, the liquid saturation distribution in the backing layer is greatly affected by the land of the current collector. The liquid saturation in the channel area of the backing layer is lower than that under the land. Since liquid water in the backing layer must be transported from the land area to the channel area for removal by channel gas, the liquid saturation in the land area must be higher in order to provide the capillary forces to this lateral liquid water motion [14]. With water generation in the cathode catalyst layer and water transport from the anode to cathode, the highest liquid saturation is about 7% in the cathode backing layer under given operating conditions. In Fig. 4, it is evident that the gradient of liquid saturation in the through-plane direction is much stronger than that in the flow direction. And, in the Plane *X*3, parallel to the membrane, the liquid saturation is lower in the channel region but rising around the edges due to the effect of the current collector lands.

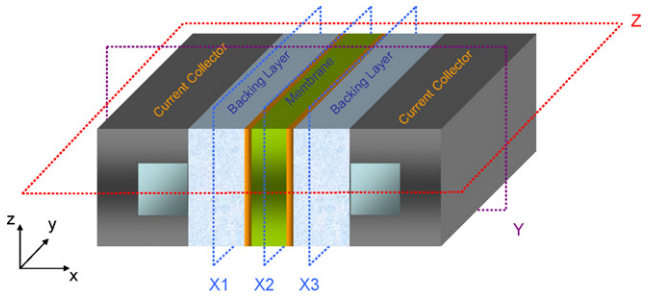

Plane	Location
X1	1/2 of anode backing thickness
X2	1/2 of membrane thickness
X3	1/2 of cathode backing thickness
Y	1/2 of cell length
Z	1/2 of cell width

Fig. 2. Illustration of 3D simulation domain and several planes for presentation of simulation results.

The net water transport coefficient contour without liquid coverage is shown in Fig. 6. In contrast with the 1D model assumption, the net water transport coefficient is found to be quite non-uniform, varying from 1.2 to −1.0. This indicates that net water transport through the membrane in the two-dimensional plane is not only from the anode to cathode, but also from the cathode to anode, depending on the location, local liquid saturation and current density. In the large middle region of the membrane, the net water transport coefficient is relatively

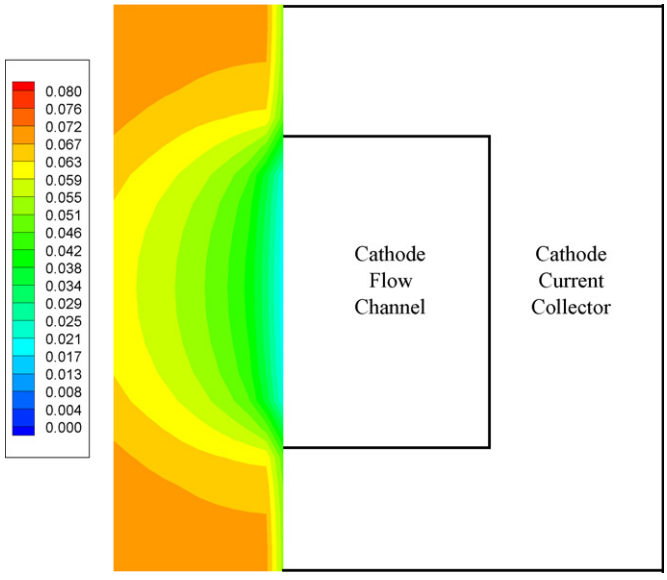

Fig. 3. Liquid saturation in the cathode backing layer of Plane *Y*, without liquid coverage.

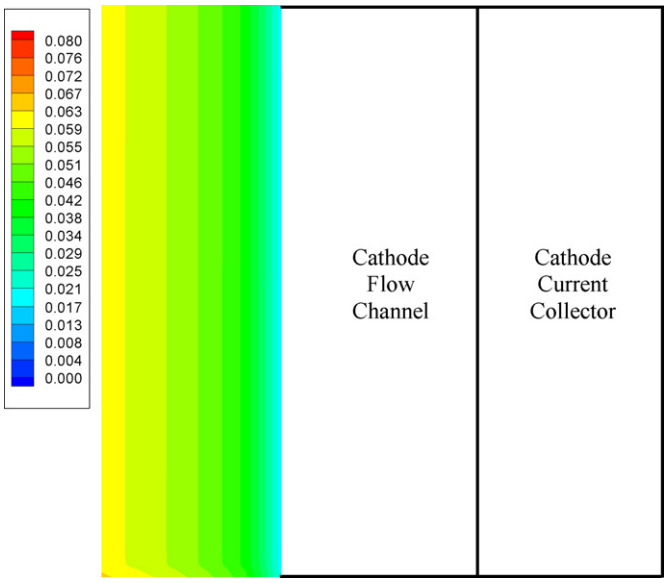

Fig. 4. Liquid saturation in the cathode backing layer of Plane *Z*, without liquid coverage.

uniform and almost constant, while it shows a large gradient and becomes even negative in the regions covered by lands.

To further investigate the reason for such a water transport coefficient distribution, water transport through the membrane due to diffusion and hydraulic permeation is shown in Fig. 7. Here, the water transport coefficients due to diffusion and hydraulic permeation are defined as $\alpha_{\text{diff}} = N^{H_2O}_{m,\text{diff}}/N^{H^+}$ and $\alpha_{\text{pl}} = N^{H_2O}_{m,\text{pl}}/N^{H^+}$, respectively. Therefore, the net water transport coefficient can be written as [10]

$$\alpha = n_d^{H_2O} + \alpha_{\text{diff}} - \alpha_{\text{pl}} \tag{7}$$

where $n_d^{H_2O}$ is the water electro-osmotic drag coefficient through the membrane, which is mainly depending on the operating temperature. It is clear that both water diffusion and hydraulic permeation have very uniform distribution in the most middle region of the membrane controlled by rather uniform current density distribution. Due to the stronger effect of hydraulic permeation from the cathode to anode through the membrane in the areas covered by lands, net water transport is pointing from cathode to anode, that is, the net water transport coefficient is negative.

Under the same operating conditions, the liquid saturation distribution in the cathode backing layer with 10% liquid coverage is shown in Figs. 8 and 9. Compared with no coverage results, the liquid saturation in the cathode backing layer is almost constant, pre-dominated by the interfacial liquid coverage of 10%. The almost constant distribution is due to the relatively large capillary diffusivity with about 10% liquid saturations in the backing layer [11]. With such a large capillary diffusivity, the liquid saturation distribution is fairly uniform in Plane *X*3 in the cathode backing layer, shown in Fig. 9. In other words, the land effect becomes negligible for the cathode liquid saturation with the interfacial liquid coverage above 10%.

The net water transport coefficient distribution with 10% liquid coverage is shown in Fig. 10. The general trend is the same as that without liquid coverage, however, with lower coefficients

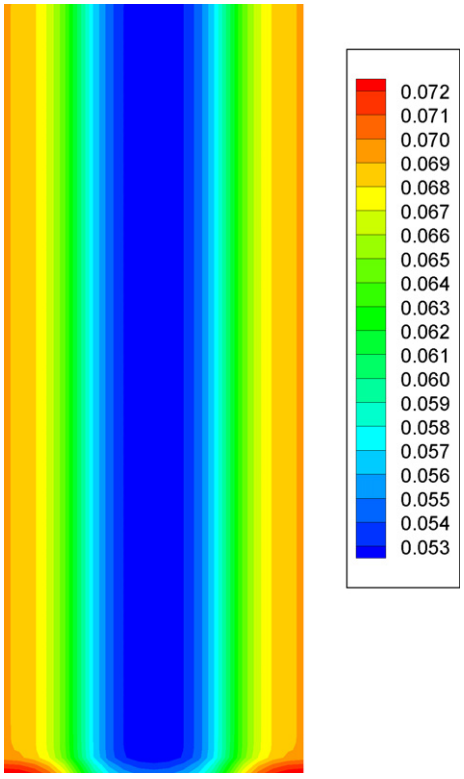

Fig. 5. Liquid saturation in cathode backing layer (Plane *X*3), without liquid coverage.

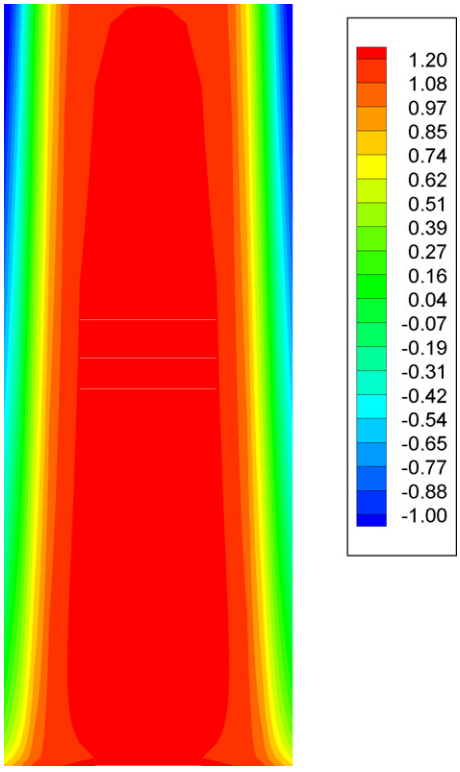

Fig. 6. Net water transport coefficient, α, distribution through the membrane, without liquid coverage.

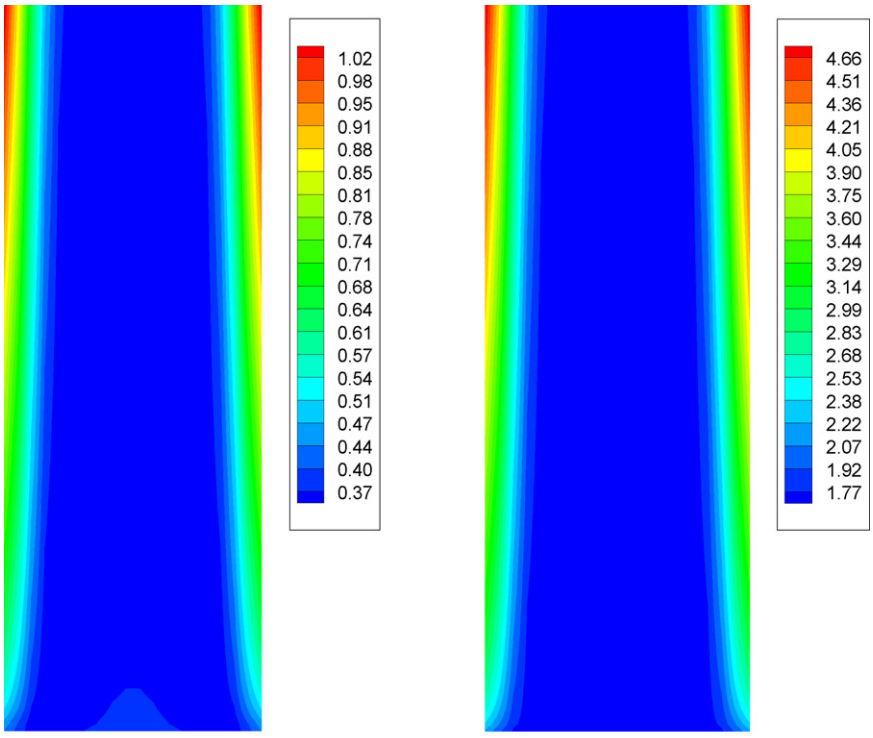

Fig. 7. Water crossover due to diffusion (a) and hydraulic permeation (b) through the membrane, without liquid coverage.

in the entire membrane region. The lower net water transport coefficient can be explained by stronger hydraulic permeation in Fig. 11(b). For both cases, water diffusion distribution from the anode to cathode is about same, while average hydraulic permeation through the membrane with 10% coverage is about 20% higher than no coverage case. Therefore, the net water transport coefficient becomes smaller with 10% liquid coverage than no coverage.

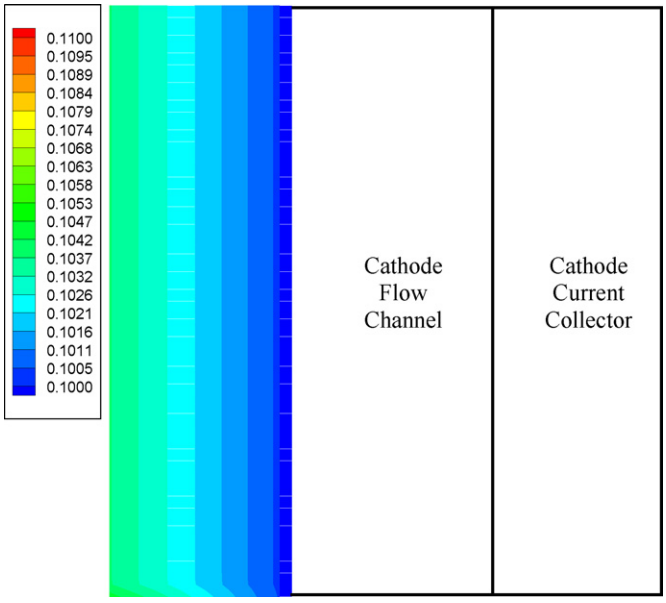

Fig. 8. Liquid saturation in the cathode backing layer of Plane *Z*, with liquid coverage of 10%.

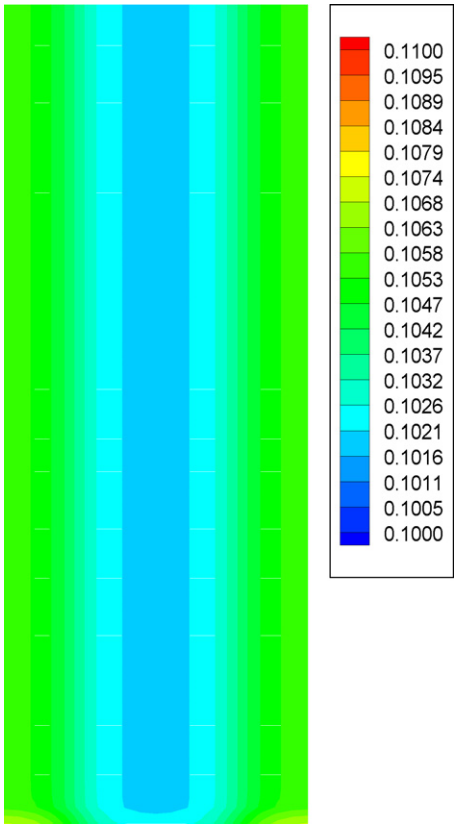

Fig. 9. Liquid saturation in the cathode backing layer (Plane *X*3), with liquid coverage of 10%.

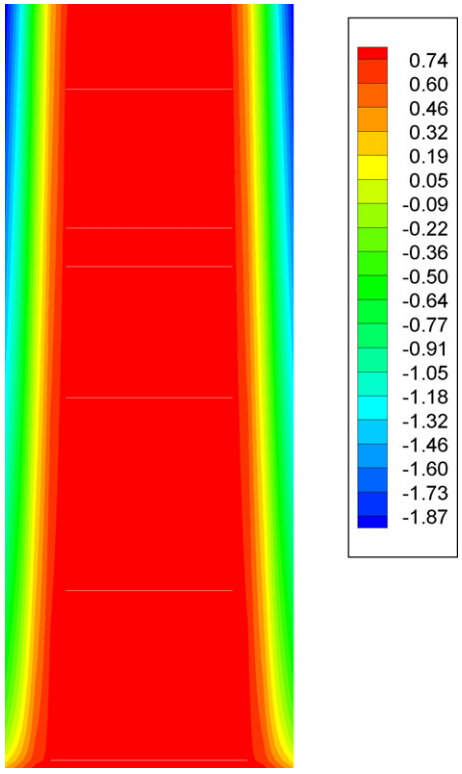

Fig. 10. The net water transport coefficient, α, distribution through the membrane, with liquid coverage of 10%.

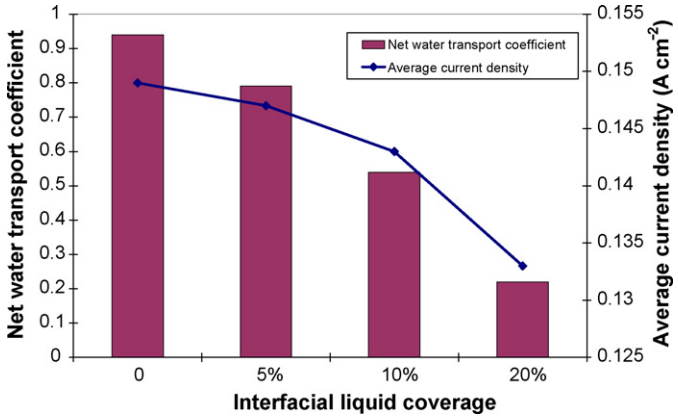

Fig. 12. Net water transport coefficients and average current densities with various liquid coverage saturations.

Using different liquid coverage saturations, the net water transport coefficients and average current densities are predicted in Fig. 12 by the 3D model. It is evident that the net water transport coefficient is highly dependant on the liquid coverage condition at the cathode backing layer surface, varying from 0.94 under the no coverage condition to 0.22 under the liquid coverage of 20%. The average current density shows relatively small variation with higher liquid coverage saturations under the given operating conditions. However, it may possibly show significant effect when oxygen transport is critical, for example, under high current density conditions or with air-breathing cathodes in portable DMFCs.

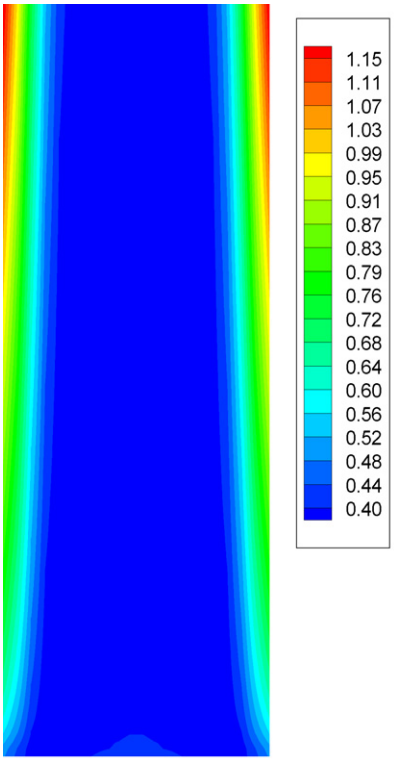

(a) By diffusion

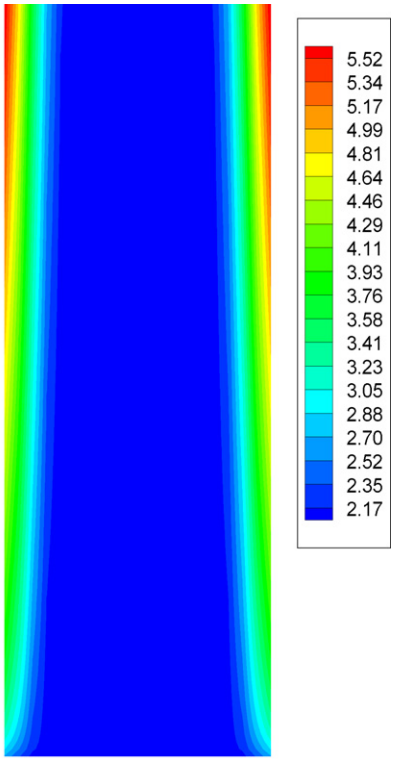

(b) By hydraulic permeation

Fig. 11. Water crossover due to diffusion (a) and hydraulic permeation (b) through the membrane with liquid coverage of 10%.

4. Conclusions

In this paper, an interfacial liquid coverage model applied at the interface between the cathode backing layer and flow channel is numerically investigated based on a 3D two-phase model, and its effects on the net water transport coefficient distribution in a DMFC are explored under typical operating conditions for portable applications. It can be seen that interfacial liquid coverage has a profound effect on the net water transport coefficient through the membrane by affecting water diffusion and hydraulic permeation. With an accurate correlation of liquid coverage from experimental measurements, water balance between the anode and cathode in the DMFC can be effectively tailored to be suitable for use of high concentration fuel, without sacrificing cell performance.

References

[1] G.Q. Lu, F.Q. Liu, C.Y. Wang, Electrochem. Solid-State Lett. 8 (2005) A1.
[2] F.Q. Liu, G.Q. Lu, C.Y. Wang, J. Electrochem. Soc. 153 (2006) A543.
[3] X. Ren, S. Gottesfeld, J. Electrochem. Soc. 148 (2001) A87.
[4] M.M. Mench, C.Y. Wang, J. Electrochem. Soc. 150 (2003) A79–A85.
[5] G.Q. Lu, C.Y. Wang, in: B. Sunden, M. Fahgri (Eds.), Transport Phenomena in Fuel Cells, WIT Press, Billerica, MA, 2004.
[6] U. Pasaogullari, C.Y. Wang, Electrochim. Acta 49 (2004) 4359.
[7] U. Pasaogullari, C.Y. Wang, J. Electrochem. Soc. 151 (2004) A399.
[8] F. Zhang, X. Yang, C.Y. Wang, J. Electrochem. Soc. 153 (2006) A225.
[9] H. Meng, C.Y. Wang, J. Electrochem. Soc. 152 (2005) A1733.
[10] W. Liu, C.Y. Wang, J. Electrochem. Soc., in press.
[11] C.Y. Wang, Chem. Rev. 104 (2004) 4727.
[12] C.Y. Wang, P. Cheng, Adv. Heat Transfer 30 (1997) 93.
[13] Z.H. Wang, C.Y. Wang, K.S. Chen, J. Power. Sources. 94 (2001) 40.
[14] Z.H. Wang, C.Y. Wang, J. Electrochem. Soc. 150 (2003) A508.
[15] X. Yang, F. Zhang, A.L. Lubaway, C.Y. Wang, Electrochem. Solid-State Lett. 7 (2004) A408.
[16] W. Liu, Methanol, Water and Heat Transport in Direct Methanol Fuel Cells for Portable Power, Ph.D. Thesis, The Pennsylvania State University, August 2005.